Elastic strings in solids: Discrete kink diffusion

C. Cattuto,[1,2] G. Costantini,[3] T. Guidi,[3] and F. Marchesoni[2,3]

[1]*Dipartimento di Fisica, Universitá di Perugia, I-06123 Perugia, Italy*
[2]*Michigan Center for Theoretical Physics, University of Michigan, Ann Arbor, Michigan 48109-1120*
[3]*Istituto Nazionale di Fisica della Materia, Universitá di Camerino, I-62032 Camerino, Italy*

The diffusive dynamics of a single discrete ϕ^4 soliton coupled to an overdamped heat bath is analyzed in detail. The Langevin equation for the soliton center of mass is derived in general form and compared with the outcome of extensive numerical simulation. The effective mass of the moving soliton must be renormalized dynamically for lattice constants of the order of its size or smaller. The corresponding mobility curve and diffusion coefficient are determined numerically: At variance with the earlier literature, discreteness effects persist even at high temperature and in the presence of strong drives.

I. INTRODUCTION

Soliton-bearing field theories have been advocated to model a variety of physical processes in particle physics,[1] soft matter such as polymers and magnetic chains,[2,3] dislocation theory,[4-6] and magnetic vortex-line dynamics.[7-9] In the continuum limit both the dynamics of a single soliton and the statistical mechanics of a dilute gas of solitons are well understood.[10,11] Discreteness, however, is an unavoidable complication, which rests upon two orders of motivations. (a) In most applications the physical system at hand is inherently discrete, namely, it reminds one more of a one- (or two-) dimensional lattice with finite constant, than of a field. This is the case of physical mechanisms that involve, for instance, linear imperfections in crystals,[12,13] and transmission arrays of either microelectronic[9,14] or biochemical bistable components.[15] (b) The numerical integration of a field equation requires necessarily the discretization of both time and space variables. This amounts to introducing an artificial lattice constant that, at variance with (a), can be varied in order to minimize uncontrolled corrections. Either way, a deeper understanding of discretization effects may help make the notion of soliton a more viable physical paradigm.

A great deal of effort has been put into the attempt at clarifying the role of discreteness in soliton dynamics. Roughly speaking the approaches brought forward so far fall into two categories. (a) Lattice field theory schemes, where the equilibrium partition function of a soliton bearing theory is computed as a function of the lattice constant and the temperature, irrespective of the actual thermalization mechanism, by means of either perturbation,[3,16] or nonperturbative techniques.[17] (b) Langevin equation (LE) schemes, where the diffusive dynamics of a single, discrete soliton is determined perturbatively either at zero,[18,19] or finite temperature, the heat bath being unspecified,[20] supplemented externally,[9] or replaced by an equilibrium phonon gas of the theory itself.[21] Both schemes aim at crafting recipes for eliminating undesirable discreteness effects, for instance, by introducing *ad hoc* counterterms,[3,17] or setting values of the temperatures, such that the residual finite-lattice corrections may be neglected.[4,5,10]

In this article we study numerically a discrete ϕ^4 theory coupled to an overdamped viscous heat bath at finite temperature—a thermalization mechanism most commonly advocated in the current literature.[5,8,22] Our main conclusion is that the diffusive dynamics of a single soliton turns out to be modified by discreteness more severely than predicted in earlier reports; such an effect persists even at high temperatures, or even in the presence of strong external driving forces, at odds with claims to the contrary. Most of the results reported here apply to the sine-Gordon (SG) chain, as well. We focused our numerical investigation on the ϕ^4 soliton because (i) no coherent chain depinning from the substrate is permitted, at variance with the SG chain,[23] (ii) no multikink solutions are allowed that, unlike the SG case, may be more stable than the relevant single kink solution.[18] Minor inconveniences are (iii) the existence of a soliton shape-mode in the continuum limit[10,11] (Sec. II A); however, in the presence of discreteness, even the SG soliton is modulated by a long-lived shape-mode.[24] (iv) Asymmetry of the minima of the tilted substrate potential; its effect is negligible in the weak drive regime (Sec. III C).

Our presentation is organized as follows. In Sec. II we derive the stationary LE for an overdamped ϕ^4 kink subjected to a random field of force at constant temperature, both in the continuum (Sec. II A) and in the discrete case (Sec. II B); the soliton thermalization question is addressed in Sec. II C. In Sec. III we simulate the deterministic dynamics of a discrete soliton in order to evaluate the lattice forces it experiences (Sec. III A) and estimate its effective mass (Sec. III B). Possible corrections to the basic treatment of Sec. II are quantified in Sec. III C and III D. In Sec. IV we simulate the stochastic dynamics of a discrete ϕ^4 kink in thermal equilibrium, with particular attention to the depinning transition from the lattice substrate (Sec. IV A) and the kink diffusion coefficient at the depinning threshold (Sec. IV B). Finally, in Sec. V we outline a summary of the results and conclusions, as well as an outlook of potential extensions of this work.

II. THE LANGEVIN EQUATION APPROACH

The LE approach to the diffusive dynamics of a single topological soliton was spurred in the mid 1980's by the

experimental observation that fluxons in long Josephson junctions execute irregular displacements reminiscent of Brownian motion.[8] Langevin equations for the soliton center of mass $X(t)$ were then construed on the basis of either phenomenological arguments,[25] or simplified energy balance equations,[22] or more systematic collective variable expansions.[19] In this section we derive the LE for a discrete topological soliton in the most general form, leaving the determination of its effective mass $\langle M_l(X) \rangle$ and substrate potential $V_{PN}(X)$ (the so-called Peierls-Nabarro potential) to an accurate comparison with the results of numerical simulation.

A. Continuum limit

Our starting point is the classical, driven ϕ^4 string described by the Hamiltonian density

$$H[\phi] = \frac{\phi_t^2}{2} + c_0^2 \frac{\phi_x^2}{2} + V[\phi] \qquad (1)$$

with on-site potential

$$V[\phi] = \frac{\omega_0^2}{8}(\phi^2 - 1)^2 - F\phi. \qquad (2)$$

The coupling of the field $\phi(x,t)$ to an equilibrium heat-bath at temperature T is represented by the last two terms on the right-hand side (RHS) of the corresponding field equation

$$\phi_{tt} - c_0^2 \phi_{xx} + \frac{\omega_0^2}{2}(\phi^2 - 1)\phi = F - \alpha\phi_t + \zeta(x,t), \qquad (3)$$

where c_0 and ω_0 are the parameters of the unperturbed ϕ^4 equation, α denotes the string damping constant and the Gaussian noise $\zeta(x,t)$ has zero mean and autocorrelation function

$$\langle \zeta(x,t)\zeta(x',t') \rangle = 2\alpha kT\delta(t-t')\delta(x-x'). \qquad (4)$$

The unperturbed $(F=0, \alpha=0)$ string bears both extended (phonons) and localized solutions (solitons).[10] Localized solutions can be well approximated to an appropriate linear superposition of moving kinks ϕ_+ and antikinks ϕ_- with

$$\phi_\pm(x,t;u) = \tanh\left(\pm\frac{x - X(t)}{2d\sqrt{1 - u^2/c_0^2}} \right), \qquad (5)$$

provided that the separation between their centers of mass $X(t) = x_0 + ut$ (x_0 and u are the integration constants), is very large compared with their size $d = c_0/\omega_0$ (dilute gas approximation). From now on we focus on the single kink (antikink) solutions (5). By inspection, $\phi_\pm$ describe a relativistic quasiparticle with energy

$$E(u) = \int H[\phi_\pm]dx = \frac{E_0}{\sqrt{1 - u^2/c_0^2}}, \qquad (6)$$

momentum $p(u) = M_0 u/\sqrt{1 - u^2/c_0^2}$, and mass

$$M_0 = \frac{E_0}{c_0^2} = \int \phi_{\pm,x}^2(x,t;u=0)dx = \frac{2}{3d}. \qquad (7)$$

The dilute gas approximation requires that $n_0(T)d \ll 1$, where $n_0(T)$ denotes the equilibrium (anti)kink density $n_0(T) \propto (1/d)\exp(-E_0/kT)$, that is $kT \ll E_0$.[10]

The phonon spectrum in the presence of a single (anti)kink consists of a continuum branch, with non-negative wave vectors k and dispersion relation $\omega^2(k) = \omega_0^2 + c_0^2 k^2$, and two discrete frequencies: the zero-frequency Goldstone mode, responsible for the soliton translation, and a shape-mode with frequency $\omega_1 = (\sqrt{3}/2)\omega_0$, describing an internal oscillation of the soliton.

The soliton LE may be best set up through a simple energy balance argument.[22] As the perturbation terms are switched on, the $\phi_\pm(x,t;u)$ energy varies according to the rate equation[7]

$$\frac{d}{dt}E(u) = \int [F - \alpha\phi_{\pm,t} + \zeta(x,t)]\phi_{\pm,t}dx. \qquad (8)$$

In order to compute the RHS of Eq. (8), we impose that the shape of the (anti)kink—i.e., the function $\phi_\mp$—remains unchanged; the only effect of the perturbation is to modify the motion of the soliton center of mass, namely, $X(t)$ and $u(t)$ must be handled as (time-dependent) stochastic processes. Simple calculations yield

$$\frac{d}{dt}E(u) = \dot{p}u, \qquad (9)$$

$$F \int \phi_{\pm,t}dx = \mp(2F)u, \qquad (10)$$

$$-\alpha \int \phi_{\pm,t}^2 dx = -\alpha pu, \qquad (11)$$

$$\left\langle \int \phi_{\pm,t}(x,t;u)\zeta(x,t)dx \cdot \int \phi_{\pm,t}(x',t';u)\zeta(x',t')dx' \right\rangle$$
$$= 2\alpha(pu)kT\delta(t-t'), \qquad (12)$$

and, on combining Eqs. (8)–(12),

$$\dot{p} = -\alpha p \mp 2F + \xi(t)\sqrt[4]{1 + (p/p_0)^2}, \qquad (13)$$

where $p_0 = M_0 c_0$ and $\xi(t)$ is a stationary Gaussian noise with zero mean and autocorrelation function $\langle \xi(t)\xi(t') \rangle = 2\alpha M_0 kT\delta(t-t')$.

The stationary probability density $P(p)$ of an undriven (anti)kink diffusing according to our LE (13) with $F=0$, can be readily derived from the Fokker-Planck formalism,[26] namely,

$$P(p) = \mathcal{N}\exp\left[-\frac{E^*(u)}{kT} \right], \qquad (14)$$

where $\mathcal{N}$ is a suitable normalization constant. The T-dependent term in

$$E^*(u) \equiv E(u) + \frac{kT}{2} \ln \left[\frac{E(u)}{E_0} \right], \qquad (15)$$

is an artifact of the energy balance argument (8). More appropriately, in Eq. (8) we ought to make use of $\mathcal{F}(u)$, the free energy of a *dressed* soliton with momentum $p(u)$—i.e., ''dressed'' with noise-induced fluctuations.[10,11] A simple iteration scheme allowed us to prove that on posing

$$\mathcal{F}(u) = E(u) \left(1 - \frac{1}{2} \frac{kT}{E(u)} \ln \left[\frac{E(u)}{E_0} \right] + \cdots \right), \qquad (16)$$

one can easily calculate the $\mathcal{O}(kT)$ corrections to the LE coefficients. In particular, the new stationary probability density $P(p)$ coincides with Eq. (14) after replacing $E^*(u)$ by $E(u)$ and, in leading order, $\langle up \rangle = kT$, as expected for a relativistic particle. These remarks, although of some relevance for assessing the self-consistency of our approach, are immaterial to the discussion of discreteness effects in Sec. III.

The momentum LE (13) can be rewritten in the standard nonrelativistic form

$$M_0 \ddot{X} = -\alpha M_0 \dot{X} \mp 2F + \xi(t), \qquad (17)$$

with $\dot{X}(t) \equiv u(t)$, under the condition that $\langle u^2 \rangle \ll c_0^2$. As from Eq. (17) $\langle u^2 \rangle = kT/M_0$, the nonrelativistic limit coincides with the dilute gas approximation $kT \ll E_0$. To make contact with the collective variable approach,[19] we note that, in view of the energy equipartition theorem, the *zero*-frequency Goldstone mode would pick up an amount $kT/2$ of thermal energy, corresponding to the average kinetic energy of the soliton.[10,11]

A final remark about the potential role of the shape mode of the ϕ^4 soliton with frequency $\omega_1 = (\sqrt{3}/2)\omega_0$.[10,11] Rice[27] has shown that the center of mass coordinate X and the internal mode ω_1 couple dynamically (at higher order), so that the propagation law for $X(t)$ develops a small periodic component with frequency ω_1; however, its amplitude is proportional to kT and, therefore, negligible in the overdamped limit.

We now summarize the range of parameter values explored in our simulation work. (i) Low temperature, $kT \ll E_0$, to ensure that kink-antikink pairs are not thermally nucleated during our observation time.[13] Accordingly, for a given temperature T, one ought to choose string lengths L such that $n_0(T)L \ll 1$. (ii) Overdamped regime, $\alpha \gg \omega_0$, to avoid relativistic effects [note that the asymptotic $\phi_\pm$ velocity in Eq. (17) is u_F with $u_F = 2F/\alpha M_0$], to suppress phonon radiation,[12,18] and to quench breather[10,18] and phonon oscillations[20,21] (of course, with the exception of the translational, or Goldstone mode[1]). (iii) Small (constant) drive, $F \ll \omega_0^2$, to preserve the bistable nature of the on-site potential $V[\phi]$ (which gets lost for $F > \omega_0^2/3\sqrt{3}$), to limit the soliton speed u_F to sub-relativistic values $u_F \ll c_0$, and to ignore the drive dependence of the soliton shape. Indeed, the minima and the barrier of $V[\phi]$ shift differently with F (Sec. III D): The corresponding tail offsets and shape deformation of $\phi_\pm$ are totally neglected in the LE approach adopted here.

B. Discrete chains

Discreteness, no matter what the cause, has a twofold effect on the soliton dynamics. (i) Phonon dressing, as it modulates the shape of the solutions (5). Upon expanding the corresponding deformation on an appropriately defined[20] basis of orthogonal discrete phonon modes, the soliton rest energy E_l turns out to be no longer translational invariant.[12] The function $E_l(X)$ becomes periodic in space with period equal to the chain constant Δx. (ii) Phonon radiation, as the moving soliton excites phonons that resonate with its modulation time constant(s).[18,19,28] The ensuing radiation damping is negligible in the overdamped regime, and will be ignored in the following.

The numerical integration of the field equation (3) was carried out by discretizing the spatial variable x, so that $\phi(i\Delta x, t) \to \phi_i(t)$, with $i = 1, 2, \ldots, N$, and Eq. (3) becomes

$$\ddot{\phi}_i - c_0^2 \Delta_2 \phi_i + \frac{\omega_0^2}{2} (\phi_i^2 - 1) \phi_i = F - \alpha \dot{\phi}_i + \zeta_i(t), \quad (18)$$

where $\Delta x = 1$, $\Delta_2 \phi_i = \phi_{i+1} + \phi_{i-1} - 2\phi_i$ and $\zeta_i(t)$ denote *local* Gaussian noise sources with $\langle \zeta_i(t) \rangle = 0$ and $\langle \zeta_i(t) \zeta_j(t') \rangle = 2\alpha kT \delta_{ij} \delta(t - t')$.

Our simulation code[23] is a framework based on Numerical Python and custom C libraries. Time integration is performed by means of a modified Mil'shtein algorithm, at finite T, and a standard fourth-order Runge Kutta for $T = 0$. For the time integration step used here, $dt = 10^{-3}$, outputs from the two integration algorithms coincide in the limit of vanishingly low temperatures.

The one-soliton bearing chain $\{\phi_i\}$ is free-end $[\phi_0 = \phi_1, \phi_{N+1} = \phi_N]$ and long enough, $L = N\Delta x$, for the diffusing soliton not to experience boundary forces. The chain extrema fluctuate around opposite $V[\phi]$ minima at any time, that is $\phi_1 = \bar{\phi}_\mp$ and $\phi_N = \bar{\phi}_\pm$, for a kink or an antikink, respectively, with $\bar{\phi}_\pm = \pm 1 + (F/\omega_0^2) \mp (3/2)(F/\omega_0^2)^2 + \cdots$. Coherent chain oscillations (with marginal effects on the soliton dynamics) may be ignored for $\alpha \gg \omega_0$.

The LE approach of Sec. II can be implemented in the discrete case, too, but with some caution. In the nonrelativistic limit, the time-dependent energy of the unbiased chain

$$E(t) = \sum_{i=1}^{N} \left[\frac{\dot{\phi}_i^2}{2} + \frac{c_0^2}{2} (\Delta \phi_i)^2 + \frac{\omega_0^2}{8} (\phi_i^2 - 1)^2 \right], \quad (19)$$

with $\Delta \phi_i = \phi_i - \phi_{i-1}$, can be approximated to[6]

$$E(t) \simeq E_l(X) + \tfrac{1}{2} M_l \dot{X}^2 \equiv E_l(\tfrac{1}{2}) + V_{\text{PN}}(X) + \tfrac{1}{2} M_l \dot{X}^2, \qquad (20)$$

where M_l is an unspecified effective soliton mass, $V_{\text{PN}}(X)$ is the Peierls-Nabarro (PN) potential[4] experienced by a free soliton moving on a periodic substrate—it vanishes in the continuum limit (17)—and $E_l(\tfrac{1}{2})$ is the minimum of the function $E_l(\delta)$, in reduced zone notation $\delta \equiv \text{Frac}[X/\Delta x]$ (see discussion of Fig. 1, below). The time derivative of $E(t)$, see Eq. (9), reads
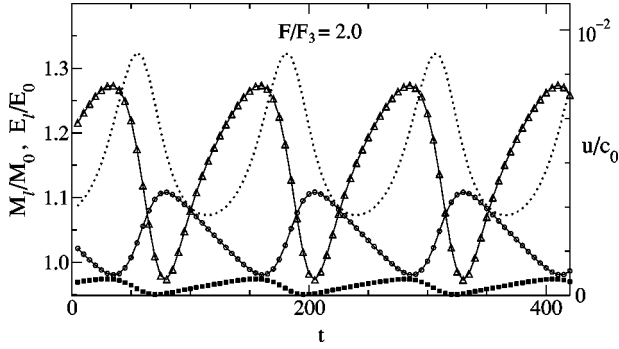
FIG. 1. Dynamical parameters of a driven kink versus time: $u(t)$ (dots), E_l/E_0 (squares), M_l/M_0, static definition (35) (circles), and M_l/M_0, dynamical definition (38) (triangles). Configurations and velocity profiles of the chain have been simulated by numerical integration of Eq. (18). Here, E_l was obtained from Eq. (19) by subtracting the kinetic energy and the average offset $(1/2)(V[\bar{\phi}_+] + V[\bar{\phi}_-])$; $u(t)$ was determined from the average velocity of the chain center of mass, $\dot{\phi}_{c.m.}$ (see Sec. III B, bottom). Note that a minimum of $E_l(t)$, in coincidence with a kink crossing the bottom of a PN well, corresponds to a maximum of the static mass and a minimum of the dynamical mass. Parameter values: $\omega_0^2 = 8$, $c_0 = 1.5$, $\alpha/\omega_0 = 10$ and $T = 0$.

$$\dot{E}(t) = \dot{X}\left[M_l \ddot{X} + V'_{PN} + \frac{\dot{X}^2}{2} M'_l \right], \qquad (21)$$

where for later convenience we retain also the last term on the RHS, although it turns out to be negligible in the nonrelativistic limit $\langle \dot{X}^2 \rangle \ll c_0^2$.

Analogously, Eqs. (10) and (11) must be replaced with

$$F \sum_{i=1}^{N} \dot{\phi}_i = \mp 2F\dot{X} \qquad (22)$$

and

$$-\alpha \sum_{i=1}^{N} \dot{\phi}_i^2 \simeq -\gamma_l \dot{X}^2, \qquad (23)$$

respectively, where

$$\frac{\gamma_l}{\gamma_0} = \frac{\sum_{i=1}^{N} \dot{\phi}_i^2}{M_0 \dot{X}^2} = \frac{K_\phi}{K_\pm}, \qquad (24)$$

with $\gamma_0 = \alpha M_0$. Here, K_ϕ and $K_\pm$ are the kinetic energy, respectively, of the entire one-soliton bearing chain $\{\phi_i\}$ and of the quasiparticle with mass M_0, associated with the soliton center of mass. Note that due to discreteness, the effective soliton mass M_l and the viscous coefficient γ_l are expected to be periodic functions of the center of mass coordinate X. In view of the $\zeta_i(t)$ correlation functions (18), the discrete version of Eq. (12) reads

$$\langle \xi(t)\xi(t') \rangle = 2\gamma_l kT \delta(t-t'). \qquad (25)$$

Finally, on inserting Eqs. (20)–(23) and (25) into the energy balance Eq. (8), we obtain for a nonrelativistic discrete ϕ^4 soliton the nonlinear LE

$$M_l(X)\ddot{X} = -\gamma_l(X)\dot{X} - \frac{\dot{X}^2}{2} M'_l(X) - V'_{PN}(X) \mp 2F + \xi(t). \qquad (26)$$

A discrete soliton is thus represented by a Brownian walker diffusing on a trapping potential; in the forthcoming section the functions $M_l(X)$, $\gamma_l(X)$, and $V_{PN}(X)$ will be investigated numerically in the *noiseless* (or zero-temperature) limit, by studying the soliton response to an applied (constant) drive F.[26]

C. Kink thermalization

We determine now under what conditions the discrete LE (31) guarantees thermalization of an undriven ($F = 0$) soliton diffusing at the string temperature T. To keep our discussion as simple as possible, we take the Smoluchowski approximation ($M_l\ddot{X} = 0$) of Eq. (26), i.e.,

$$\gamma_l(X)\dot{X} = -\frac{\dot{X}^2}{2} M'_l(X) - V'_{PN}(X) + \xi(t). \qquad (27)$$

As for an equilibrium dilute gas, $\langle \dot{X}^2 \rangle = kT/M_l$, Eq. (27) can be further approximated to

$$\gamma_l(X)\dot{X} = -\frac{kT}{2} \frac{d}{dX} \ln M_l(X) - V'_{PN}(X) + \xi(t). \qquad (28)$$

The corresponding Fokker-Planck equation[26] can be written down readily and solved for the stationary probability density $P(X)$, that is

$$P(X) = \mathcal{N}\sqrt{\gamma_l(X)} \exp\left(-\frac{V_{PN}(X)}{kT} - \frac{1}{2}\ln[M_l(X)] \right), \qquad (29)$$

where $\mathcal{N}$ is a suitable normalization constant. Thermalization requires that $\gamma_l(X) \propto M_l(X)$; hence, in the nonrelativistic limit,

$$P(X) = \mathcal{N}\exp\left(-\frac{V_{PN}(X)}{kT} \right), \qquad (30)$$

as from the canonical formalism. In the following, thermal fluctuations, if any, are taken so small that $\mathcal{O}(kT/E_0)$ corrections may be neglected. The linear version of the LE in Eq. (26),

$$M_l\ddot{X} = -\gamma_l\dot{X} - V'_{PN}(X) \mp 2F + \xi(t), \qquad (31)$$

thus provides an adequate framework to interpret our simulation data.

III. DISCRETE DYNAMICS

The periodic LE coefficients $M_l(X)$, $\gamma_l(X)$, and $V_{PN}(X)$ can be determined to a large accuracy by comparison with numerical simulation. Actually, a number of perturbation schemes have been developed[6] to compute analytically the

coefficients of the Fourier series for $M_l(X)$ and $V_{PN}(X)$. Despite a considerable mathematical effort, at this time there appear to persist substantial discrepancies among theoretical predictions by different authors[20,29,30] and between theory and simulation[30] (for a review see Ref. 6).

In a preliminary report[31] we showed that the relation

$$\gamma_l(X) = \alpha M_l(X), \qquad (32)$$

is verified numerically for a discrete chain too (see also Sec. III B). This result, in addition to ensuring thermalization of the soliton dynamics (Sec. II C), makes the phenomenological quantity $M_l(X)$, introduced in Eq. (20), expressible, in principle, as a ratio of chain sums. Moreover, for a travelling soliton, the spatial modulation of $M_l(X)$ turns out to be relatively unimportant (at least for not too small a d value[19,20]), so that $M_l(X)$ may be replaced with its time average $\langle M_l(X) \rangle$. In conclusion, on neglecting $\mathcal{O}(kT/E_0)$ corrections, the number of unspecified LE coefficients is reduced to two, only, namely, the X-dependent PN potential and an appropriate soliton effective mass.

A. The Peierls-Nabarro potential

Our ansatz is the assumption, to be assessed *a posteriori* (Sec. III C), that the PN potential is dominated by its first spatial Fourier component[20]

$$V_{PN}(X) = \frac{k_{PN}}{4\pi^2}[1 + \cos(2\pi X)]. \qquad (33)$$

Then we plotted the instantaneous configurational energy E_l [computed through Eq. (19) after subtracting the chain kinetic term and correcting for the soliton offsets $\bar{\phi}_\pm$, see Fig. 1] versus time for a soliton in the running state, i.e., driven with nonvanishing speed $u(t)$: E_l oscillates between a minimum E_{min} and a maximum E_{max}, that do not depend on the actual (small) value of the drive. The choice of F, though, affects the time dependence of $u(t)$ in a manner reminiscent of a damped particle falling down a tilted washboard potential.[26] Furthermore, we computed the rest energies $E_l(\frac{1}{2})$ and $E_l(0)$ statically at $F=0$. It turns out that the damped soliton, no matter what the initial speed, gets trapped midway between sites, $\delta = 1/2$, with energy $E_l(\frac{1}{2}) = E_{min}$. On the other hand, one can pin the soliton at $X = i\Delta x$, or $\delta = 0$, and observe that the energy $E_l(0)$ of the pinned solution coincides with E_{max}. Hence, the static determination of the PN potential amplitude $k_{PN}(d)/4\pi^2 = (E_{max} - E_{min})/2$.

In Fig. 2 the ratios $E_l(\frac{1}{2})/E_0$, $E_l(0)/E_0$, and $k_{PN}/\bar{k}_{PN}$ are plotted for increasing values of the soliton size d. As d gets much larger than Δx, discreteness effects tend to vanish, i.e., $E_l \to E_0$ and $k_{PN} \to 0$. In the opposite limit, $d \to 0$, Eq. (19) yields $E_l(\frac{1}{2})/E_0 = 3d$ and $E_l(0)/E_0 = 3/16d$; analogously, for $\bar{k}_{PN} \equiv k_{PN}(0)$ we obtain $\bar{k}_{PN} = (\pi^2/4)\omega_0^2$.

Finally, we investigated the unlocking transition that takes place as F increases above the threshold value $F_3 = k_{PN}/4\pi$. As shown by Risken[26] for the cosine potential (33), the time
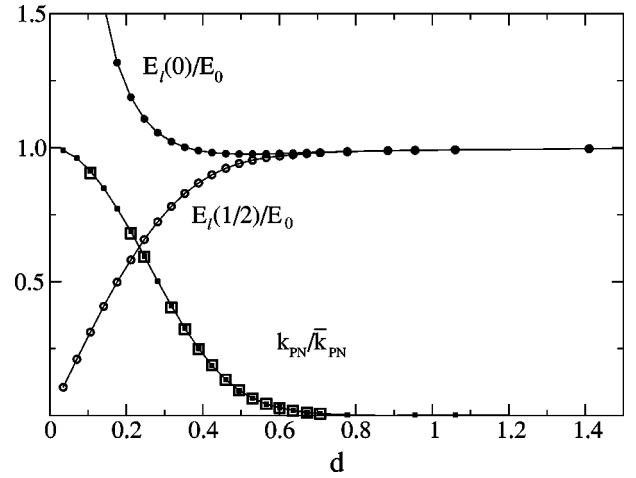
FIG. 2. Characterization of the PN potential. The static quantities $E_l(\frac{1}{2})/E_0$ (open circles) and $E_l(0)/E_0$ (solid circles) are plotted versus d. The difference $E_l(0) - E_l(\frac{1}{2})$, in units of $\omega_0^2/8$ (solid squares), is compared with $k_{PN}/\bar{k}_{PN}$, as obtained from the fitting law (34) (open squares). The agreement is very close for $d > 0.2$. Parameter values: $\omega_0^2 = 8$, $\alpha/\omega_0 = 10$ and $T = 0$; F was chosen larger than, but close to F_3 (see text).

average $u(F) \equiv \langle u(t) \rangle$ tends to an asymptotic value u_l (analyzed in Sec. III B) according to the zero-temperature law

$$\frac{u(F)}{u_l} = \sqrt{1 - \left(\frac{F_3}{F}\right)^2} \qquad (34)$$

for $F \gtrsim F_3$ and $u(F) = 0$, otherwise. As pointed out in Sec. II A, in the continuum limit $u(F) = u_F$ with $u_F = 2F/\gamma_0$. The curves of $u(F)/u_F$ versus F (Fig. 3) illustrate well the
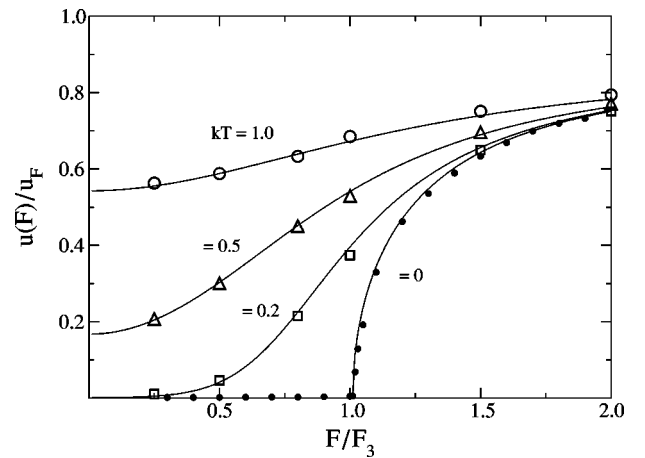
FIG. 3. The kink mobility $u(F)/u_F$ versus F/F_3 for $kT = 0$ (solid circles); $= 0.2$ (squares); $= 0.5$ (triangles); $= 1.0$ (open circles) (in units of $k_{PN}/4\pi^2$). The kink velocity $u(F)$ has been obtained by numerical integration of Eq. (18), see text. The threshold F_3 is identified with $k_{PN}/4\pi$ and plotted in Fig. 2. The solid curves represent the relevant Risken's solution [Eq. (11.78) in Ref. 26, or Eq. (34) at $T = 0$]. As we chose to rescale $u(F)$ by u_F, Risken's solutions have been divided by the fitting parameter u_F/u_l reported in Fig. 4. Parameter values: $\omega_0^2 = 8$, $c_0 = 1.5$ and $\alpha/\omega_0 = 10$.

discreteness-induced trapping mechanism mentioned in the earlier literature[12,18–20] and afford an independent determination of both k_{PN} and u_l. This provides us with a dynamical measurement of the PN potential amplitude: The agreement between our alternate estimates of k_{PN}, is verified within a 1% accuracy in Fig. 2, deviations being expected at small d, due to the asymmetry of the tilted potential $V[\phi]$ (see Sec. III D). In fact, the maximum value of k_{PN} accessible to a driven (anti)kink is $(16/3\pi\sqrt{3})\bar{k}_{PN}$, because for $F > \omega_0^2/3\sqrt{3}$ the chain becomes unstable.[31] Note that, for $F > F_3$ the profile of $V_{PN}(X)$ could have been determined directly, by combining the ''trajectories'' of $E(t)$ and $u(t)$ numerically, see Fig. 1.

B. The kink effective mass

We discuss now the renormalized parameters γ_l and M_l of the Brownian soliton (31). These parameters control the diffusive properties of the fluctuating soliton at finite temperature. Strictly speaking, in the overdamped regime, $\alpha \gg \omega_0$, our LE approach gives us direct access to two quantities, only, the temperature T and the viscous coefficient γ_l (24), as $M_l\ddot{X}\simeq 0$ (Smoluchowski approximation).

Numerical fits of the curves $u(F)/u_F$ in the suprathreshold neighborhood $F\gtrsim F_3$, based on the zero-temperature law (34), provide a rather accurate estimate of u_l as a function of d. In view of our ansatz (33), $u(F)/u_F$ must be compared with the RHS of Eq. (34) divided by the fitting parameter u_F/u_l. Unfortunately, we could not explore the domain $d < 0.2$, lest the threshold F_3 grows so large that the soliton deformation caused by the drive can no longer be neglected [and Eq. (34) must be modified as explained in Sec. III D]. Moreover, we computed numerically the RHS of Eq. (24) and observed that it oscillates with time; γ_l is actually a periodic function of the soliton position with *minima* at $\delta = 1/2$. As the definition of u_l involves the time average of the instantaneous velocity $u(t)$, it seems quite reasonable to pose $u_l=2F/\langle\gamma_l\rangle$ and compare u_F/u_l with $\langle\gamma_l\rangle/\gamma_0$, as we did in Fig. 4. The agreement is very close, thus lending further evidence to our LE picture of the discrete one-soliton dynamics. It should be remarked at this point, that discretization may affect through $\langle\gamma_l\rangle$ most simulations of thermal pair nucleation too.[2,13]

The question of an independent determination of M_l could be tackled for instance in the underdamped diffusion regime, $\alpha\ll\omega_0$, at the cost of large radiation effects.[12,18] Alternately, one could study the oscillations of a trapped, frictionless soliton around a minimum of the PN potential,[30] or rely on a collective variable scheme.[19,20] Indications are that a viable *static* definition of M_l would be

$$M_l=\sum_{i=1}^{N}(\Delta\phi_i)^2. \tag{35}$$

Direct computations show a marked X−dependence of M_l with *maxima* midway between sites (Fig. 5). This result is certainly true in the high discreteness limit, as for $d\to 0$ the extrema of $M_l(X)$ are $M_l(\frac{1}{2})=4$ and $M_l(0)=2$, respec-
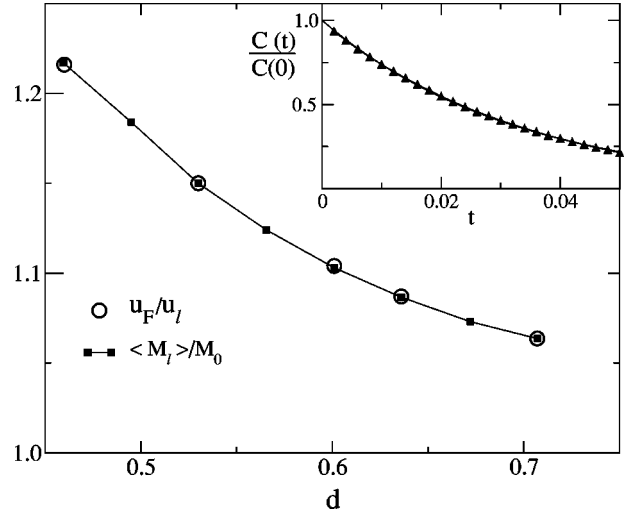
FIG. 4. The kink damping question. The fitting parameter u_F/u_l (open circles) is plotted versus d and compared with $\langle\gamma_l\rangle/\gamma_0(=\langle M_l\rangle/M_0)$ (Eq. (38), squares) also as a function of d. Parameter values $\omega_0^2=8$, $\alpha/\omega_0=10$, and $T=0$. Inset: subtracted autocorrelation function (36)—from numerical integration of Eq. (18)—and its exponential fit $C(t)=C(0)e^{-\alpha t}$ for $kT=k_{PN}/4\pi^2$. Other parameter values: $\omega_0^2=8$, $c_0=1.5$, $\alpha/\omega_0=10$, and $F=F_3$.

tively. Surprising are, indeed, conflicting predictions, for instance in Refs. 19,20, based on the notion of ''bare'' soliton mass. As a matter of fact, Fig. 1 shows that, again at variance with Refs. 19,20, also the dc component of $M_l(X)$ is strongly affected by discreteness. However, the time-averaged mass $\langle M_l\rangle$ deviates from its continuum limit M_0 by an amount that does not suffices to explain alone the numerical values of $\langle\gamma_l\rangle/\gamma_0$ plotted in Fig. 4; actually, not even its maximum $M_l(\frac{1}{2})$ shown in Fig. 5, would do it.[31] Therefore, using $\langle M_l\rangle$ from definition (35) for the renormalized mass of the discrete soliton, would require introducing simultaneously a renormalized damping constant $\alpha_l\equiv\langle\gamma_l\rangle/\langle M_l\rangle$ in place of α.
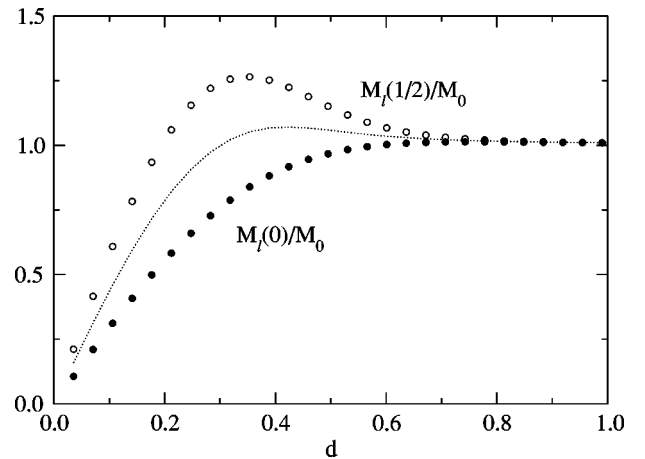
FIG. 5. The static mass (35) of a kink at rest at the bottom and the top of a PN substrate: $M_l(\frac{1}{2})/M_0$ (open circles) and $M_l(0)/M_0$ (solid circles) are plotted versus d. For the sake of a comparison, we also display the arithmetic average of the two quantities (dotted curve). Parameter values: $\omega_0^2=8$, $\alpha/\omega_0=10$, and $T=0$.

In order to test this possibility we computed the subtracted autocorrelation function of the kink velocity $u(t)$,

$$C(t-t') \equiv \lim_{t,t' \to \infty} [\langle u(t)u(t')\rangle - \langle u(t)\rangle\langle u(t')\rangle] \quad (36)$$

(see Fig. 4, inset) at finite temperature T and large but *finite* damping constant. Such a damping regime is well described by the so-called $1/\alpha$ expansion,[26] which goes beyond the Smoluchowski approximation (corresponding to $\alpha = \infty$) of the relevant LE; accordingly, one expects that $C(t-t')/C(0) = \exp[-\alpha(t-t')]$, with $C(0) = kT/\langle M_l\rangle$. The numerical value α_{num} fitted through our simulation data agrees with the input value α within less than 1%.[32] This result rules out the notion of renormalized damping constant α_l. An alternate definition of soliton effective mass is suggested by Eq. (24), namely,

$$\frac{1}{2}M_l\dot{X}^2 \equiv \sum_{i=1}^{N} \frac{\phi_i^2}{2}. \quad (37)$$

Such a *dynamical* definition of M_l replaces the static definition (35) with the advantage that both the chain $\{\phi_i\}$ and the soliton $\phi_\pm$ have the same damping constant α. The two definitions of the kink effective mass are contrasted in Fig. 1: A maximum of the static mass corresponds to a minimum of the dynamical mass, and vice versa.

For computational purposes, definition (37) can be conveniently rewritten as

$$M_l = 4\frac{\displaystyle\sum_{i=1}^{N} \dot{\phi}_i^2}{\left(\displaystyle\sum_{i=1}^{N} \dot{\phi}_i\right)^2}. \quad (38)$$

Here we made use of the equality $u(t) = (N/2)\dot{\phi}_{c.m.}(t)$, that relates the velocity of the kink to that of the chain center of mass, $N\dot{\phi}_{c.m.} = \sum_{i=1}^{N} \dot{\phi}_i$; Eq. (38) is certainly valid in the absence of thermal fluctuations ($T=0$) and phonon disturbances ($\alpha \gg \omega_0$). An alternate technique for computing $u(t)$ is discussed at the top of Sec. IV.

C. The librational frequency

Our determination (37) of the kink mass applies implicitly to the driven case, where the soliton propagates at a finite average speed $u(F)$. In the absence of an external drive, $F=0$, a discrete kink gets trapped between two adjacent chain sites and undergoes damped oscillations (depending on its initial conditions) until it comes to a halt. Under such circumstances, Boesch *et al.*[30] proposed to indentify $\langle M_l\rangle$ with the static mass (35) at $\delta = \frac{1}{2}$, namely, with its *maximum* value $M_l(\frac{1}{2})$.

Following this indication we measured the oscillation (or "librational") frequency of an *underdamped* kink trapped at the bottom of a PN well. To do this, we took α and N small and tilted the potential $V[\phi]$ with $F \ll F_3$; after the chain reached equilibrium, the tilt was removed instantaneously: The chain starts oscillating around the symmetric $V[\phi]$
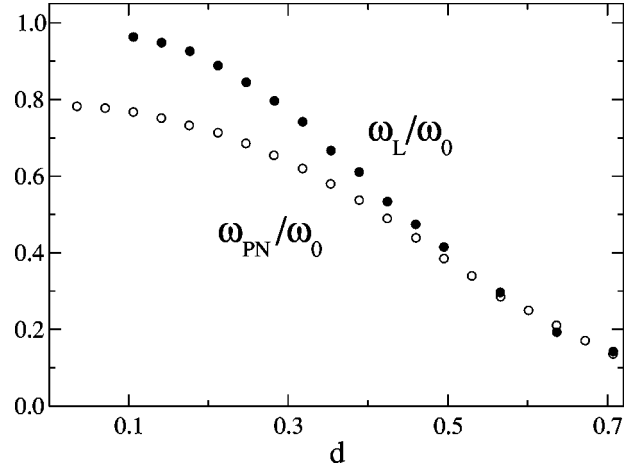
FIG. 6. The librational frequency of a trapped kink: ω_L/ω_0 (solid circles) was determined numerically by integrating Eq. (18), see text; ω_{PN}/ω_0 (open circles) is computed from the definition $\omega_{PN}^2 = k_{PN}/M_l(\frac{1}{2})$, with $k_{PN}(d)$ and $M_l(\frac{1}{2})$ plotted in Figs. 2 and 5, respectively. Parameter values $\omega_0^2 = 8$, $\alpha/\omega_0 = 10^{-2}$, $N = 40$, and $T = 0$.

minima, $\phi = \pm 1$, with angular frequency ω_0, whereas the kink oscillates inside the trap with librational frequency ω_L, smaller than ω_0. Of course, for $c_0 \to 0$ (strong discreteness limit) ω_L must tend to ω_0.[30] The velocity of the chain center of mass $\dot{\phi}_{c.m.}$ has been recorded and Fourier transformed to extract its periodic components with frequencies ω_0 and ω_L. [The discrete phonon spectrum $\omega^2(i) = \omega_0^2 + 4c_0^2 \sin(\pi i/2N)$, with $i = 1, \ldots, N$, and the onset of the shape mode ω_1 have been also resolved.[12,19]] In Fig. 6 the ratio ω_L/ω_0 is compared with the corresponding estimate ω_{PN}/ω_0 based on the ansatz (33) for $V_{PN}(X)$. The frequency ω_{PN} is defined through $\omega M_l(\frac{1}{2})$, where $k_{PN}(d)$ is taken from the data set of Fig. 2 and $M_l(\frac{1}{2})$ is the static mass of the trapped kink plotted in Fig. 5. Note that in the limit $d \to 0$, k_{PN} and $M_l(\frac{1}{2})$ tend to $(\pi^2/4)\omega_0^2$ and 4, respectively, hence $\omega_{PN}/\omega_0 \to \pi/4$.

We make now an important remark. In the foregoing Section we have proven that our definition (37) for the kink mass is more accurate than definition (35) employed in Ref. 30 and here, above; however, Eq. (38) clearly shows that the limit $M_l(\frac{1}{2}) = 4$ for d tending to zero, holds for both definitions. This allows us to interpret the unexpected discrepancy between ω_L (measured directly) and ω_{PN} (derived for a sinusoidal PN potential) as a confidence test of our ansatz (33). Following the more refined approaches of Refs. 19,20, let us consider the next-to-leading component of the spatial Fourier expansion of $V_{PN}(X)$, that is,

$$V_{PN}(X) = \frac{k_{PN}}{4\pi^2}[1 + \cos(2\pi X) - \kappa \cos(4\pi X)]. \quad (39)$$

Accordingly, the correction parameter $\kappa(d)$ reaches its maximum for $d = 0$, where it must obey two simple constraints: $V_{PN}(0) - V_{PN}(\frac{1}{2}) = \omega_0^2/8$ (see Sec. III A) and $V''_{PN}(\frac{1}{2})/M_l(\frac{1}{2}) = \omega_0^2$. Solving for $\kappa(0)$ yields $\kappa(0) = 4/\pi^2 - (1/4) \simeq 0.15$.

This is an estimate of the maximum error introduced by our ansatz for $V_{PN}(X)$. Finally, we notice that the κ corrections to the maximum slope of the PN potential Eq. (39), which in turn is proportional to the depinning threshold F_3, are $\mathcal{O}(\kappa^2)$, only. This explains the close agreement between static and dynamical measurements of k_{PN}, even at the lowest d values reported in Fig. 2.

D. Asymmetry effects

In Sec. III A the PN amplitude has been computed in two alternate ways: On assuming for $V_{PN}(X)$ the sinusoidal form (33), we have related k_{PN}, first, to the rest-energy difference $E_l(0) - E_l(\frac{1}{2})$ of an undriven kink, $F=0$, and, then, to the depinning threshold F_3. In Fig. 2, static and dynamical determinations of k_{PN} appear to coincide with one another within the accuracy of our numerics, thus corroborating the conclusion that the PN substrate experienced by the soliton center of mass, is independent of F over most of the drive interval. [It can be easily proven that corrections to $V_{PN}(X)$ contribute to the order $(F/\omega_0^2)^3$ or higher, only, and make the PN wells asymmetric.]

The same conclusion does not apply to the overall dynamics of the soliton. Under the action of a positive, small tilt, $F \ll \omega_0^2$, the curvatures $\omega_\pm^2$ of the ϕ^4 potential (2) around its right ($\bar{\phi}_+$) and left ($\bar{\phi}_-$) minimum split off with $\omega_\pm^2 = \omega_0^2[1 \pm 3(F/\omega_0^2) - 3(F/\omega_0^2)^2 + \cdots]$. Simultaneously, the center of the soliton shifts to a distance $a_\pm = 1 \pm 3(F/\omega_0^2) - (3/2)(F/\omega_0^2)^2 + \cdots$ from the stable points $\bar{\phi}_\pm$, respectively.

Thus, a finite tilt, $F \neq 0$, causes an *asymmetric* spatial deformation of the soliton—not accounted for explicitly in our derivation of the LE (31)—that results eventually in a drive dependence of its effective mass $\langle M_l \rangle$. As a consequence, we expect that u_l/u_F, too, depends on F, so that the fitting law (34) may not level off at a horizontal asymptote. To avoid such an inconvenience, in Fig. 3 we restricted the fitting procedure to the rising branch of the mobility curve, immediately above the depinning threshold F_3; accordingly, the fitted values of $\langle M_l \rangle / M_0$ reported in Fig. 4 have been obtained at $F = F_3+$, namely, for an applied drive that increases with decreasing d.

The effects of the F dependence of $\langle M_l \rangle$ are illustrated explicitly in Fig. 7, where the kink mobility curve, $u(F)/u_F$, is plotted for two choices of d, representing the continuum and the discrete regime, respectively. For large d values the kink runs freely along an almost continuous chain; its mobility, however, slants upwards, slightly above the expected asymptote $u(\infty)/u_F = 1$. A simple interpretation of this result takes into account the kink deformation in the tilted potential (2). The mass of the tilted soliton may be approximated to

$$\frac{\langle M_l \rangle}{M_0} = \frac{a_+^2}{2}\left(\frac{\omega_+}{\omega_0}\right) + \frac{a_-^2}{2}\left(\frac{\omega_-}{\omega_0}\right), \qquad (40)$$

whose reciprocal is plotted in Fig. 7 for a comparison.

For smaller soliton sizes, the mobility curve does not converges to a horizontal asymptote, either. Nevertheless, the
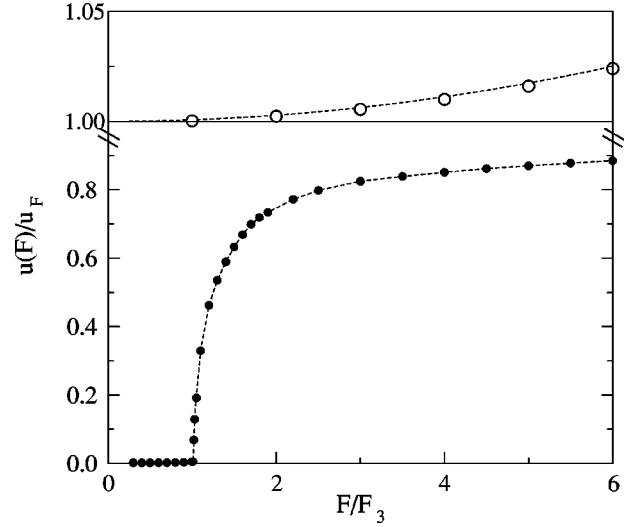
FIG. 7. Asymmetry corrections to the mobility curve $u(F)/u_l$ for $c_0 = 40$ (dashed curve and data points above the solid line) and $c_0 = 1.5$ (dashed curve and data points below the solid line). The data points (open and solid circles) have been computed by numerical integration of Eq. (18), following the technique in Sec. III B. In the discrete regime, $c_0 = 1.5$, the dashed curve is the fitting law (34), with $u_l = 2F/\alpha\langle M_l \rangle$ and M_l computed from Eq. (38). For $c_0 = 40$, the dashed curve represents the continuum limit $u(F)/u_F = M_0/\langle M_l \rangle$ (see the text) with $\langle M_l \rangle / M_0$ approximated as in Eq. (40). The solid line, corresponding to $u = u_F$, was drawn for graphical convenience. Other parameter values $\omega_0^2 = 8$, $\alpha/\omega_0 = 10$, and $T = 0$.

validity of the fitting law (34) can be extended to the entire range of interest, provided that u_l/u_F, or $M_0/\langle M_l \rangle$, be computed explicitly from Eq. (38) as a function of F. The outcome of the improved fitting procedure of Fig. 7 is very encouraging, indeed: The asymmetry effects due to the drive F can be fully incorporated in the framework of our LE approach.

IV. KINK DIFFUSION

So far, we have determined the LE coefficients $\langle M_l(X) \rangle$ and $V_{PN}(X)$ by simulating the deterministic response of the coordinate $X(t)$ to an external forcing term. Relying on the results of Sec. III, we are now in the position to interpret our simulation data for the termal diffusion of a single soliton along a discrete ϕ^4 chain. At this point, no further parameter can be fitted to the numerics; the LE (31) alone, complemented with relations (32), (33) and (37), should suffice to reproduce the temperature dependence of both the mobility curve and the diffusion coefficient of a diffusing (overdamped) soliton.

As an introductory note, we remind that the identity $u = (N/2)\dot{\phi}_{c.m.}$ of Sec. III B fails in the presence of persistent fluctuations and could hardly be used to locate a randomly diffusing soliton. We developed a more efficient computational technique to sample the stochastic process $X(t)$: At regular time intervals Δt_X copies of the chain configuration are recorded and then fed through a filtering routine that
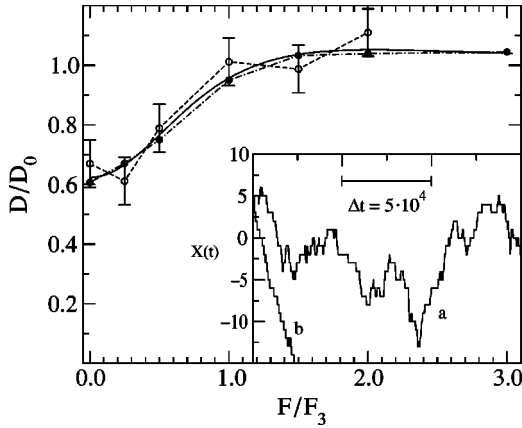
FIG. 8. Diffusion coefficient $D(F)$ of a single kink versus F for $\omega_0^2 = 8$, $c_0 = 1.5$, $\alpha/\omega_0 = 10$, and $kT = k_{PN}/4\pi^2$ (open dots with error bars). The quantity $D_0 = kT/\alpha\langle M_l\rangle$ has been computed by making use of definition (38) for the kink mass. The solid curve represents prediction (42) as obtained numerically from Risken's solution for the mobility curve $u(F)/u_F$ in Fig. 3. For the sake of a comparison, we simulated also the diffusion of a driven Brownian particle described by LE (31) with fixed damping constant α and mass $\langle M_l\rangle$ (solid circles); the PN potential (33) and the mass $\langle M_l\rangle$ were taken to coincide with the relevant discrete chain values fitted in Figs. 3 and 4 Inset: samples of the $X(t)$ trajectories for $F=0$ (a) and $F = 0.1$. (b) The quantization of X due to our kink positioning technique is apparent. The kink residence times in the PN wells are distributed according to an exponential law.

makes the chain evolve further in time, but at zero temperature and much larger a damping constant; as a result, the chain converges quickly to a static configuration with the (anti)kink located between two adjacent chain sites. This corresponds to filtering out any phonon oscillation, possible discrete breathers[6] and thermal fluctuations; the ensuing quantization (with unit step) of the sampled soliton trajectory $X_n = X(n\Delta t_X)$ (see Fig. 8, inset) has no bearing on the statistics of our simulations, provided that the displacements measured are conveniently long and Δt_X is chosen shorter than any relevant time scale in the problem.

A. Depinning transition

In Fig. 3 the soliton mobility is plotted versus F at finite, but low temperatures, $kT \lesssim k_{PN}/4\pi^2$. Our simulation data for $u(F,T)/u_F$ match very closely the corresponding Risken's solution, also displayed for reader's convenience—it took as little as summing up the continued fraction expansion (11.78) of Ref. 26. In particular, the suprathreshold values of $u(F,T)/u_F$ do not change much with the temperature, even when kT is raised clear above $k_{PN}/4\pi^2$ (half the PN barrier height), and approach the value $\gamma_0/\langle\gamma_l\rangle$ obtained in the noiseless case of Sec. III B. This remark conforms well to our picture of a diffusing discrete soliton as of a massive quasiparticle undergoing (driven) Brownian motion in a periodic, nonfluctuating potential $V_{PN}(X)$, with effective mass $\langle M_l\rangle$, (37), and equilibrium temperature T. In particular, as anticipated in Sec. II C, finite temperature corrections to $\langle M_l(X)\rangle$ and $V_{PN}(X)$ are negligible for $kT \ll E_0$ Moreover,

the fits in Fig. 3 support the conclusion that the dynamical role of discreteness does not fade away at high temperatures, nor does for strong driving forces F, at odds with common knowledge.

B. Diffusion coefficient

The soliton response to an external force F is customarily expressed in terms of its mobility, i.e., a stationary observable that may be averaged over time according to the ergodic hypothesis.[26] In the present section we pursue an alternative approach: We focus on the spatial dispersion of the soliton center of mass $X(t)$ along the driven discrete chain. As the soliton runs with average speed $u(F)$ in the direction of the external force F, the random switches between locked and running state are expected to cause an additional diffusion effect on the particle around its average position $\langle X(t)\rangle$. To this purpose we computed numerically the *normal* diffusion coefficient

$$D = \lim_{t\to\infty} \frac{1}{2t}\langle[X(t)-\langle X(t)\rangle]^2\rangle \tag{41}$$

of the transport process (31) and studied D as a function of the bias F at constant temperature. In Fig. 8 we display our results for D/D_0, where the quantity $D_0 = kT/\alpha\langle M_l\rangle$ denotes Einstein's diffusion coefficient for the free Brownian motion in one dimension.[32] A bump in the curves of D versus F is detectable for $F \sim F_3$, with $D(F) > D_0$; the depinning threshold is thus characterized by an excess diffusion.[33]

The F dependence of the diffusion coefficient in the overdamped regime $\alpha \gg \omega_0$ can be interpreted analytically in the framework of the linear response theory. On extending the approach developed by Risken[26] for the zero bias case, one derives an approximate law that relates the mobility of a biased Brownian particle to its diffusion coefficient, that is,[33]

$$\frac{D}{D_0} = \frac{u(F)}{u_l} + F\frac{d}{dF}\left[\frac{u(F)}{u_l}\right]. \tag{42}$$

The bump in the $D(F)$ curve of Fig. 8 is thus related to the jump of $u(F)/u_l$ at the depinning threshold. In Fig. 8 the simulation data for a diffusing discrete ϕ^4 kink are compared with the theoretical prediction (42) and the simulation data for an equivalent Brownian particle (31), with PN potential (33) and averaged coefficients (32) and (38). Within the statistics of our data, the agreement is very close.

More notably, the same quantitative agreement has been obtained over the entire drive and temperature range we have explored in Fig. 3. At lower temperatures the subthreshold diffusion process is apparently dominated by the interwell hopping mechanism [and formula (42) becomes less and less accurate];[33] longer and longer residence times come into play, that eventually exceed our computing capabilities. Finally, Eq. (42) in the zero drive case, $F=0$, leads to the simple formula $D(F)/D_0 = u(F)/u_l$;[26] we checked such a prediction successfully for the three kT values reported in Fig. 3.

V. CONCLUSIONS

A single soliton diffusing along a discrete ϕ^4 chain is well described as a nonrelativistic, massive particle executing Brownian movement on a periodic substrate modeled by a PN potential. Discreteness affects the inertial properties of the soliton, for which we have introduced a dynamical definition of effective mass, and the profile of the PN potential, closely fitted by its first two Fourier components. On the contrary, the two quantities that determine the coupling of the chain to its heat bath, are insensitive to discreteness: soliton temperature and damping constant coincide, indeed, with those of the chain, as desirable in thermal equilibrium.

The Brownian motion of a single (anti)kink obeys a linear LE, whose coefficients have been related phenomenologically to chain sums. This approach, while not completely self-consistent, has the great advantage of providing a simple recipe for interpreting quite accurately the results of numerical simulations, and in principle, of experiments on actual physical systems. On combining a few simple measurementes, one can fine-tune the coefficients of the soliton LE; a full statistical description of the thermal diffusion of a single soliton (and, possibly, of the entire chain) follows immediately. Such a procedure allowed us to detect certain discrepancies in the more self-consistent collective variable treatments published in the recent literature.

A number of related problems would deserve further investigation.

(1) *Underdamped regime.* We remind that all of the above applies to an overdamped chain, only, where phonons are suppressed altogether. On decreasing the string damping constant, both the nonrelativistic limit and our LE derivation, explicitly based on neglecting phonon damping, become untenable (phonon *radiation damping* starts playing an important role[18,19,28]): Soliton diffusion is then likely to be better describable as a nonstationary stochastic process, for which, however, the phenomenology available to-date is still rather poor.[6,12,20]

(2) *Phonon spectrum of a one-soliton bearing chain.* Discreteness affects both the spectrum and the density of the normal modes in a ϕ^4 chain.[12] Our simulation shows that the librational ω_L and the shape-mode frequency ω_1, shift to opposite directions with increasing d. Moreover, internal modes are known[24,34] to bifurcate from the phonon essential band $\omega(i)$ in thresholdless fashion, i.e., extra modes may appear as soon as the continuum string $\phi(x,t)$ is modeled through the discrete chain $\phi_i(t)$, no matter what d. Furthermore, localized nonlinear solutions (also termed discrete breathers) show up for vanishingly small α values.[35]

(3) *Collisional dynamics.* Discreteness affects the soliton scattering off another soliton or a chain defect, as well.[6] As a consequence, the kink-antikink pair nucleation rates[13] ought to be computed to account for the trapping action of the PN potential. Analogously, the soliton-impurity interaction is likely to be effectively screened by the PN substrate. Finally, as discrete solitons are not transparent to propagating phonons, one might consider the possibility of phonon mediated soliton-soliton interactions.[28]

(4) *Periodic forcing.* At zero (or low) damping the ac driven dynamics of a single discrete soliton might reveal resonant behaviors due to the frequency matching between internal modes and the periodic shape modulation of the soliton travelling on a PN substrate.[36] Asymmetry in the presence of a tilt, $F \neq 0$, might also support ratchetlike soliton transport.[37]

[1] R. Rajaraman, *Solitons and Instantons* (North-Holland, Amsterdam, 1982), and references therein.

[2] M. Remoissenet, *Waves Called Solitons* (Springer, Berlin, 1994).

[3] R.K. Dodd, J.C. Eilbeck, J.D. Gibbon, and H.C. Morries, *Soliton and Nonlinear Equations* (Academic Press, London, 1982).

[4] A. Seeger and P. Schiller, in *Physical Acoustics*, edited by W.P. Mason (Academic, New York, 1966), Vol. III A, p. 361.

[5] J.P. Hirth and J. Lothe, *Theory of Dislocations* (Wiley, New York, 1982), Chap. 8.

[6] O.M. Braun and Yu.S. Kivshar, Phys. Rep. **306**, 1 (1998), and references therein.

[7] D.W. McLaughlin and A.C. Scott, Phys. Rev. A **18**, 1652 (1978).

[8] M. Salerno, E. Joergensen, and L.R. Samuelsen, Phys. Rev. B **30**, 2635 (1984).

[9] S. Watanabe, H.S.J. van der Zant, S.H. Strogatz, and T.P. Orlando, Physica D **97**, 429 (1996).

[10] J.F. Currie, J.A. Krumhansl, A.R. Bishop, and S.E. Trullinger, Phys. Rev. B **22**, 477 (1980).

[11] T. Tsuzuki and K. Sasaki, Prog. Theor. Phys. (Suppl.) **94**, 72 (1988).

[12] J.F. Currie, S.E. Trullinger, A.R. Bishop, and J.A. Krumhansl, Phys. Rev. B **15**, 5567 (1977).

[13] F. Marchesoni, C. Cattuto, and G. Costantini, Phys. Rev. B **57**, 7930 (1998).

[14] F. Marchesoni, L. Gammaitoni, and A.R. Bulsara, Phys. Rev. Lett. **76**, 2609 (1996).

[15] M. Löcher *et al.*, Phys. Rev. E **61**, 4954 (2000).

[16] R.E. de Leonardis and S.E. Trullinger, Phys. Rev. A **10**, 2603 (1974); and Phys. Rev. B **22**, 4558 (1980).

[17] J.M. Speight, Nonlinearity **12**, 1373 (1999).

[18] M. Peyrard and D. Kruskal, Physica D **14**, 88 (1984).

[19] R. Boesch, C.R. Willis, and M. El-Batanouny, Phys. Rev. B **40**, 2284 (1989), and references therein.

[20] C. Kunz and J.A. Combs, Phys. Rev. B **31**, 527 (1985); J.A. Combs and S. Yip, *ibid.* **28**, 6873 (1983).

[21] F. Marchesoni and C.R. Willis, Europhys. Lett. **12**, 491 (1990).

[22] F. Marchesoni, Phys. Lett. A **115**, 29 (1986).

[23] C. Cattuto and F. Marchesoni, Phys. Rev. Lett. **79**, 5070 (1997).

[24] R. Boesch and C.R. Willis, Phys. Rev. B **42**, 2290 (1990).

[25] L. Gunther and Y. Imry, Phys. Rev. Lett. **44**, 1225 (1980); M. Büttiker and R. Landauer, *ibid.* **46**, 75 (1981).

[26] H. Risken, *The Fokker-Planck Equation* (Springer, Berlin, 1984), Chap. 11.

[27] M.J. Rice, Phys. Rev. B **28**, 3587 (1983).

[28] C. Cattuto, G. Costantini, T. Guidi, and F. Marchesoni (unpublished).

[29] Y. Ishimori and T. Munakata, J. Phys. Soc. Jpn. **51**, 3367 (1982).

[30] R. Boesch and C.R. Willis, Phys. Rev. B **39**, 361 (1989).

[31] T. Guidi, C. Cattuto, and F. Marchesoni (unpublished).

[32] Thus, for $\alpha \to \infty$, the velocity autocorrelation function $C(t-t')$ tends to $D_0 \delta(t-t')$, with $D_0 = kT/\alpha \langle M_l \rangle$, as to be expected. Note that beyond the linear approximation of Sec. II A, D_0 may develop corrections $\mathcal{O}(kT/E_0)^2$ and higher. See, e.g., N.R. Quintero, A. Sánchez, and F.G. Mertens, Phys. Rev. E **60**, 222 (1999); J. Dziarmaga and W. Zakrzewski, Phys. Lett. A **251**, 193 (1999).

[33] G. Costantini and F. Marchesoni, Europhys. Lett. **48**, 491 (1999).

[34] Y.S. Kivshar *et al.*, Phys. Rev. Lett. **80**, 5032 (1998); P.G. Kevrekidis and C.K.R.T. Jones, Phys. Rev. E **61**, 3114 (2000).

[35] S. Flach and C.R. Willis, Phys. Rep. **295**, 181 (1998).

[36] N.R. Quintero, A. Sánchez, and F.G. Mertens, Phys. Rev. E **62**, 5695 (2000); Phys. Rev. Lett. **84**, 871 (2000).

[37] F. Marchesoni, Phys. Rev. Lett. **77**, 2364 (1996); A.V. Savin, G.P. Tsironis, and A.V. Zolotaryuk, Phys. Rev. E **56**, 2457 (1997).